



全天时便携式户外型红外探测气溶胶激光雷达系统设计及应用

庄鹏 谢晨波 康宝荣 刘建明 夏小维

Design and application of all-day portable outdoor infrared detection aerosol lidar system

Zhuang Peng, Xie Chenbo, Kang Baorong, Liu Jianming, Xia Xiaowei

在线阅读 View online: <https://doi.org/10.3788/IHLA20230636>

您可能感兴趣的其他文章

Articles you may be interested in

扫描式气溶胶激光雷达研制与观测研究

Development and observational studies of scanning aerosol lidar

红外与激光工程. 2018, 47(12): 1230009 <https://doi.org/10.3788/IHLA201847.1230009>

大气气溶胶污染监测中应用的新型全天时户外型拉曼-米散射激光雷达系统

New all-weather outdoor Raman-Mie scattering lidar system used in atmospheric aerosol pollution monitoring

红外与激光工程. 2019, 48(7): 706001 <https://doi.org/10.3788/IHLA201948.0706001>

户外型探测臭氧和气溶胶激光雷达系统研制

Outdoor lidar system for measurement of ozone and aerosol profiles

红外与激光工程. 2019, 48(7): 706008 <https://doi.org/10.3788/IHLA201948.0706008>

基于积分球分光与接收的透射式能见度测量系统

Transmission measurement system for visibility based on integrating sphere applied to light splitting and receiving

红外与激光工程. 2018, 47(10): 1017003 <https://doi.org/10.3788/IHLA201847.1017003>

气溶胶消光系数反演PM_{2.5}质量浓度方法研究

Research on inversion method of PM_{2.5} mass concentration by aerosol extinction coefficient

红外与激光工程. 2020, 49(S2): 20200367 <https://doi.org/10.3788/IHLA20200367>

北京2014年冬季边界层高度与颗粒物浓度的相关性研究

Correlation study on boundary layer height and particulate matter concentration at Beijing in winter 2014

红外与激光工程. 2018, 47(7): 717007 <https://doi.org/10.3788/IHLA201847.0717007>

全天时便携式户外型红外探测气溶胶激光雷达 系统设计及应用

庄 鹏^{1,2}, 谢晨波³, 康宝荣², 刘建明², 夏小维^{4*}

- (1. 铜陵学院 电气工程学院, 安徽 铜陵 244061;
2. 安徽蓝科信息科技有限公司, 安徽 合肥 230031;
3. 中国科学院安徽光学精密机械研究所 中国科学院大气光学重点实验室, 安徽 合肥 230031;
4. 巢湖学院 机械工程学院, 安徽 合肥 238000)

摘要: 介绍了全天时便携式户外型红外探测气溶胶激光雷达的工作原理、系统设计与多种场景应用分析。红外探测气溶胶激光雷达具有大气穿透性强,受天空背景光影响小、对大粒子敏感等特点,在大气气溶胶污染时空分布特征获取、水平能见度监测和垂直边界层监测的应用上取得较好的效果。系统水平扫描可获取大区域颗粒物分布图,及时发现污染源并联合近地面风速风向、颗粒物和一氧化碳浓度等数据评估污染源影响程度,同时能够准确地反演水平能见度,与标准能见度仪比对相对误差均小于 20%。激光雷达反演边界层高度采用消光系数梯度法,实验结果与探空气球反演绝对偏差为 200 m,能够准确反演边界层高度。该系统能够实时精确地捕获大气气溶胶分布与传输情况,准确反演水平能见度、边界层高度等信息,在大气监测领域具有广泛的应用场景。

关键词: 红外气溶胶激光雷达; 颗粒物分布; 能见度; 边界层

中图分类号: TN958.98

文献标志码: A

DOI: 10.3788/IRLA20230636

0 引言

我国大气污染治理经过几十年的探索与实践取得了显著的成就。随着大气环境探测技术的不断进步和发展,近年来我国环境监测领域通过自主研发和技术引进推出了大量高端环境监测设备和技术手段,实现了天地空一体化、多参数、多尺度,从总量特征到组分特征的高精度监测,进一步通过融合信息化建设中万物互联、信息共享的特点打造智慧监管平台,有效实现“人机”结合,践行科学治污、精准治污的精细化管理需求,为大气污染的有效治理和空气质量持续提升提供了有力保障。

激光雷达作为一种主动遥感仪器,是目前对流层内大气气溶胶立体分布特征监测的利器。美国 NASA 于 1993 年首次研制成功微脉冲激光雷达^[1],克

服了传统雷达高能量、高消耗等缺点,而我国于 2001 年由中国科学院安徽光学精密机械研究所首次研制成功,具有便携性好、探测范围广、时空分辨率高等优点,目前已广泛应用于气环境监测、空气质量管理和气象预报等领域^[2]。激光雷达可弥补现有地面监测数据空间分布率的不足^[3],主要采用水平、垂直、走航、组网多种监测模式^[4],其中水平扫描能有效监测水平能见度^[5],动态提取污染源位置和传输路径^[6];垂直监测可分析气溶胶垂直扩散、沉降传输及光学特征时空变化^[7-8],边界层变化及其云信息^[9]、沙尘监测^[10]等。现有系统,微脉冲激光雷达普遍采用 532 nm 波长,而穿透性强、隐秘性好的 1064 nm 不可见红外波长在气溶胶地基式观测种应用相对较少,多应用于卫星搭载^[11],中国海洋大学^[12]、西安理工大学^[13]曾有过

收稿日期:2023-11-03; 修订日期:2023-12-27

基金项目:安徽省自然科学基金项目(2208085UQ03);中国科学院合肥大科中心协同创新培育基金项目(2022HSC-CIP025);巢湖学院人才项目(KYQD-2023056)

作者简介:庄鹏,男,工程师,博士,主要从事大气激光雷达探测技术方面的研究。

通讯作者:夏小维,女,博士生,主要从事大气激光雷达探测技术数据分析方面的研究。

相关研究,但缺乏实际监测应用。文中介绍了一种自主研发的红外激光雷达,在环境污染及多元突变天气条件下,可实时对气溶胶分布、能见度、边界层高度进行检测,对分析污染气团扩散、沉降变化趋势具有独特的优势,在观测需求越来越高的大背景下,能够为环境管理决策、气象服务提供更科学有效的数据支撑。

1 探测原理

米散射激光雷达方程^[14]的反演方法是获取大气气溶胶垂直或水平分布的关键。Fernald 法将分子散射和气溶胶散射分开来考虑,理论上反演过程更加严谨,因此得到了广泛应用。其反演过程如下:

$$\beta(R) = \beta_m(R) + \beta_a(R) \quad (1)$$

式中: $\beta(R)$ 为大气分子后向散射系数和气溶胶粒子的后向散射系数之和; $\beta_m(R)$ 为距离 R 处大气分子后向散射系数; $\beta_a(R)$ 为距离 R 处大气气溶胶后向散射系数。

$$\alpha_a(R) = -S_a/S_m \alpha_m(R) + \frac{R^2 P(R) \exp\left[2(S_a/S_m - 1) \int_R^{R_c} \alpha_m(r) dr\right]}{\frac{R_c^2 P(R_c)}{\alpha_a(R_c) + S_a/S_m \alpha_m(R_c)} + 2 \int_R^{R_c} r^2 P(r) \exp\left[2(S_a/S_m - 1) \int_R^{R_c} \alpha_m(r) dr\right] dr} \quad (5)$$

$$\alpha_a(R) = -S_a/S_m \alpha_m(R) + \frac{R^2 P(R) \exp\left[2(S_a/S_m - 1) \int_R^{R_c} \alpha_m(r) dr\right]}{\frac{R_c^2 P(R_c)}{\alpha_a(R_c) + S_a/S_m \alpha_m(R_c)} + 2 \int_{R_c}^R r^2 P(r) \exp\left[2(S_a/S_m - 1) \int_{R_c}^R \alpha_m(r) dr\right] dr} \quad (6)$$

$$\alpha_m(R) = 9.807 \times 10^{-23} \times \frac{273}{T(R)} \times \frac{P_a(R)}{1013} \left(\frac{1}{\lambda \times 10^{-7}} \right)^{4.0117} \quad (7)$$

式中: $T(R)$ 为大气分子的温度随高度 R 的变化; $P_a(R)$ 为大气分子的压强随高度 R 的变化; λ 为激光发射波长。

$T(R)$ 与 $P_a(R)$ 可通过 1976 年美国标准大气模型得到。从公式中可以看出,由于已假设了分子和气溶胶的消光后向散射比,且由大气模式可得出分子的消光系数边界值,只要在探测路径上获取参考距离 R_c 处的气溶胶消光系数边界值,即可得出探测路径上任意距离的消光系数。由于现阶段气溶胶激光雷达的时间和空间分辨率基本达到了秒级和米级,因此,上述算法不局限于垂直探测,在水平探测时也可

$$\alpha(R) = \alpha_m(R) + \alpha_a(R) \quad (2)$$

式中: $\alpha(R)$ 为大气分子消光系数和气溶胶消光系数之和; $\alpha_m(R)$ 为距离 R 处大气分子消光系数; $\alpha_a(R)$ 为距离 R 处大气气溶胶消光系数。

定义气溶胶的消光后向散射比为:

$$S_a = \frac{\alpha_a(R)}{\beta_a(R)} \quad (3)$$

定义分子消光后向散射比为:

$$S_m = \frac{\alpha_m(R)}{\beta_m(R)} \quad (4)$$

式中: S_m 的值一般认为是常数 $8\pi/3$ 。

根据激光雷达方程,经过积分、取自然对数以及求导等运算后,得到参考高度 R_c 处以下各高度上的气溶胶消光系数如公式(5)所示。 R_c 处以上各高度的气溶胶消光系数如公式(6)所示。参考高度 R_c 一般选取不含气溶胶的清洁大气层所在的高度。大气中分子的尺度谱和密度等分布相对比较稳定,因此,分子的消光系数可根据美国标准大气分子模式较为精确地确定,如公式(7)所示。

认为高度方向在小尺度范围内大气均匀。

2 系统介绍

在 355、532、1064 nm 三个波长同步观测实验中发现,1064 nm 波长因更接近气溶胶粒子直径,更加符合米散射探测理论,所以对气溶胶粒子更加敏感。从图 1 中可以看出,1064 nm 对探测气溶胶垂直分布结构更为有利,结构非常丰富,非常适合于气溶胶、云、团雾探测。相反,355 nm 波长更利于探测大气分子信号,对大颗粒气溶胶粒子不敏感,回波信号更趋向于分子模式。而 532 nm 波长介于两者之间,从图中可以看出气溶胶结构,但不明显。因此,选择 1064 nm 波长开展气溶胶观测实验。

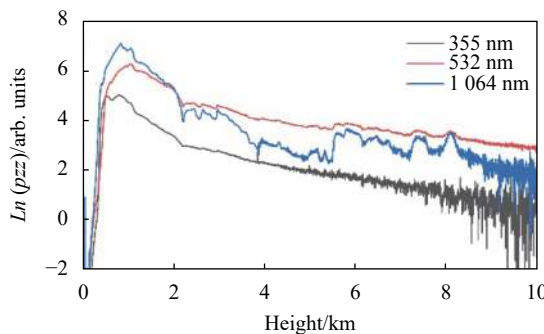


图1 355、532、1064 nm 信号强度廓线

Fig.1 Signal intensity profiles of 355 nm, 532 nm, 1064 nm

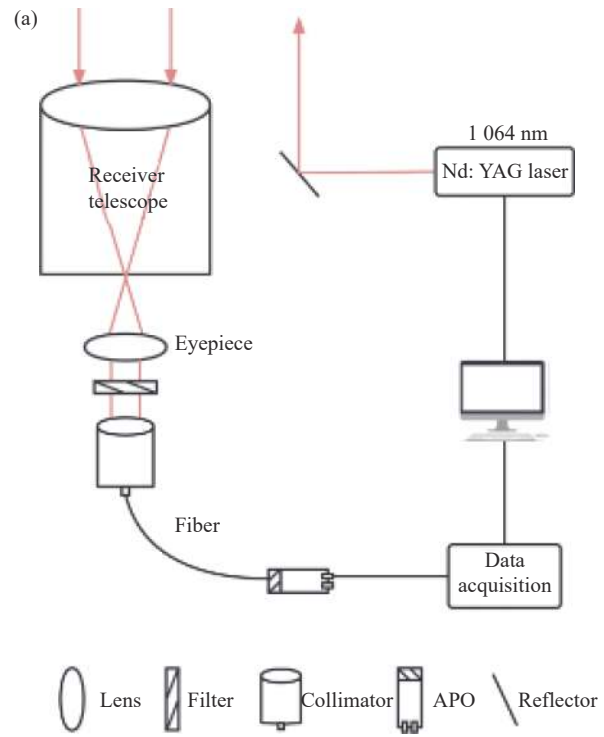
图2为气溶胶激光雷达产品结构示意图和外观图。系统主要由激光发射单元、光学接收单元、数据采集与处理单元三部分组成,其主要的技术指标参数如表1所示。采用Nd:YAG激光器的基频1064 nm线偏振激光作为探测光源,望远镜采用非球面透镜作为主镜,非球面透镜具有像差小和焦距短的优点,可以减小接收模块体积,后继光学与探测单元采用光纤耦合装置和小芯径多模光纤组成,可以有效控制望远镜接收视场。光学通道测量1064 nm出射激光与大气中粒子作用产生的米散射信号,利用通道的测量数据并结合上述反演方法便可得到对流层气溶胶和云光学参数分布特征。

表1 红外气溶胶激光雷达系统主要技术参数

Tab.1 Technical parameters of infrared aerosol lidar

Parameter	Value
Wavelength/nm	1064
Repetition frequency/kHz	3
Single-pulse energy/ μ J	150
Telescope calibre/mm	≥ 100
Detection distance/km	15
Vertical height resolution/m	7.5
Time resolution/s	1-600
Equipment weight/kg	≤ 30
Blind spot distance/m	≤ 100
Weight/kg	20
Volume/mm	470×250×280
Operation temperature/°C	-30-55
Protective class	IP65

激光雷达是一种光学精密仪器,尤其是户外运行



(a)



图2 (a) 红外气溶胶激光雷达产品结构示意图;(b) 红外气溶胶激光雷达产品外观图

Fig.2 (a) Lidar product structure of infrared aerosol; (b) Lidar product appearance of infrared aerosol

需要兼顾抗高低温、防盐雾和光路稳定等因素。首先,设备内部按照小型化、功能化和模块化原则进行布局,包括激光发射、接收、信号探测和采集以及运行控制等部分。这些部分之间通过冗余连接来增强互换性和光机稳定性。其次,根据热源热量进行内部

循环和传导散热设计,选择耐高低温材料和传热材料,例如使用铝散热片将激光器和工控机的热量传导至设备外部,并增加风扇和保温材料以确保内部空气均匀流通。最后,根据 IP65 防护等级进行防尘和防盐雾结构设计,例如采用密封结构和在望远镜处采取双重密封措施等。经过综合优化设计和运行测试,通过了中国气象局装备许可证考核。

3 应用个例分析

3.1 颗粒物水平扫描监测应用个例分析

2022 年 10 月至 2023 年 3 月,在某市国家城市环境空气质量监测站点(甲站点)附近布置红外激光雷达,红外激光雷达对以该站点为圆心、半径为 5 km 的

圆形区域进行 360°水平扫描监测,雷达采用 24 h 连续不间断扫描方式,以正西方向为起点顺时针扫描,并设置扫描周期为 30 min,得到激光雷达水平扫描完整一圈图谱,从而分析不同污染点源产生的时间及其位置信息,获取城市区域内污染分布情况,以及城市污染输送通道。

通过分析 2022 年 10 月至 2023 年 3 月期间该国控站点气溶胶激光雷达的水平扫描监测结果,共发现 10 处主要污染源区域如图 3 所示,各污染源的出现频次统计如表 2 所示,结果表明,污染源主要分布在雷达点位的东南侧和东北侧,污染源 A、污染源 B 和污染源 C 等 3 处污染源为出现频次偏高的污染源。

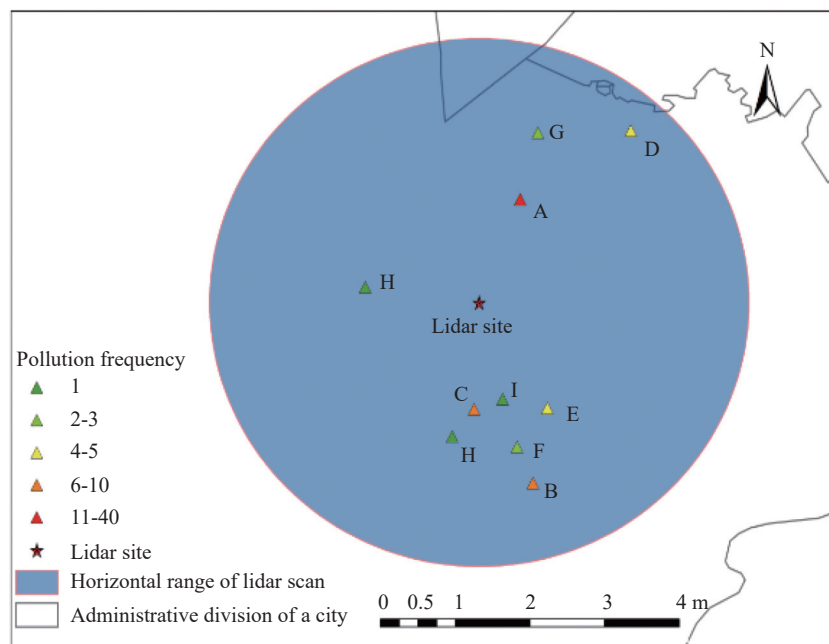


图 3 红外激光雷达水平扫描监测污染源分布情况

Fig.3 Distribution of pollution sources monitored by infrared lidar horizontal scanning

以 2023 年 2 月 5 日监测结果为例,某市国家城市环境空气质量监测站点(甲站点)颗粒物小时浓度与市平均颗粒物浓度对比结果如图 4 所示,晚间 19:00-20:00,该国控点颗粒物浓度显著高于城市平均值,其中 20:00 该站点 PM₁₀ 浓度为 134 μg/m³,而城市 PM₁₀ 浓度均值仅为 79 μg/m³;同时间段一氧化碳(CO)站点浓度与城市平均浓度变化图如图 5 所示,其浓度值同

样有所升高,初步判读具有一处污染排放特征^[15]。

图 6 为 2 月 5 日 19:00-20:00 红外激光雷达水平扫描监测图谱结果,其中图谱中空白部分为激光雷达水平扫描时受周围建筑遮挡区域,缺失角度范围为 50°,该区域无数据。从激光雷达监测结果可以发现,2 月 5 日 19:00 至 20:00,雷达扫描监测到一处明显消光系数高值^[16],位置为污染源 A 附近区域,该时段内

表2 红外激光雷达扫描监测污染源结果统计情况

Tab.2 Statistical results of infrared laser radar horizontal scanning to monitor pollution sources

Number	Source location	Frequency of pollution/times
1	A	40
2	B	10
3	C	9
4	D	5
5	E	4
6	F	3
7	G	2
8	H	1
9	I	1
10	J	1

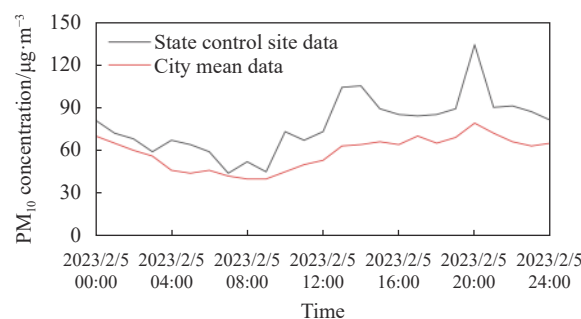


图4 2月5日某市颗粒物浓度变化图

Fig.4 Time variation of particulate matter concentration on February 5

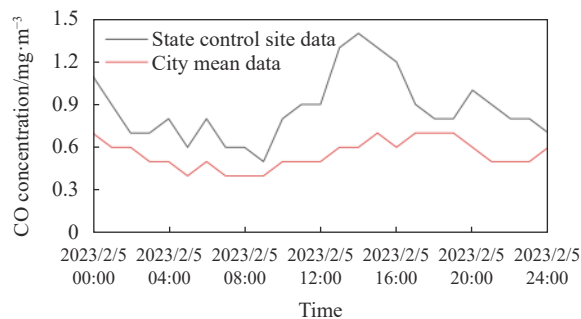


图5 2月5日某市一氧化碳浓度变化图

Fig.5 Time variation of CO concentration on February 5

地面主导风向为东北风,风速等级为2级,该污染源所产生污染物在东北风作用下,向西南方向扩散,而该国控空气站点在该污染源A下风向。综合分析可以判断出,5日晚间,污染源A附近区域持续产生污染物,在东北风作用下造成位于下风向的国控空气站点的颗粒物浓度以及CO浓度数据同步升高,受污染

区域范围由北至南呈扩大趋势。

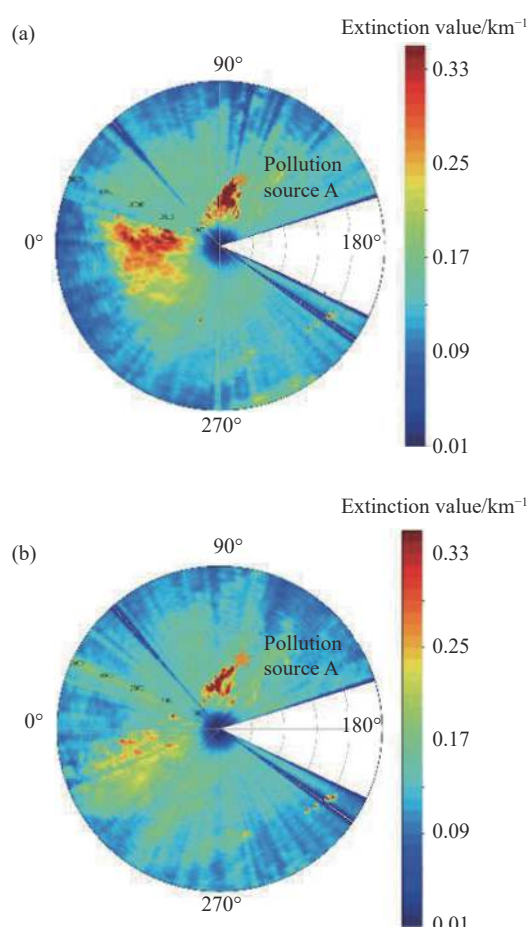
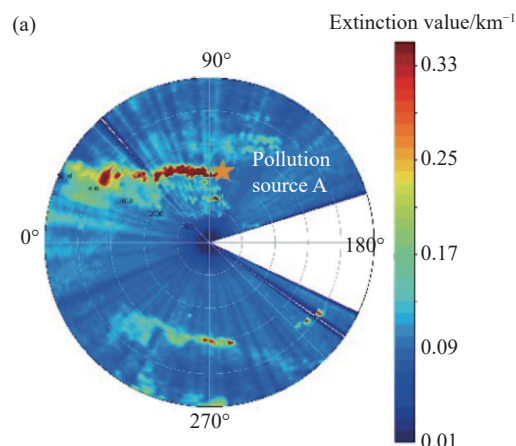


图6 红外气溶胶激光雷达扫描监测结果(2月5日 19:00-20:00)

Fig.6 Scanning and monitoring results of infrared aerosol lidar(February 5, 19:00 to 20:00)

2月3日19:00-20:00红外激光雷达水平扫描监测图谱结果图7所示,近地面站点颗粒物、一氧化碳浓度分别与其城市均值的时间序列图如图8、图9



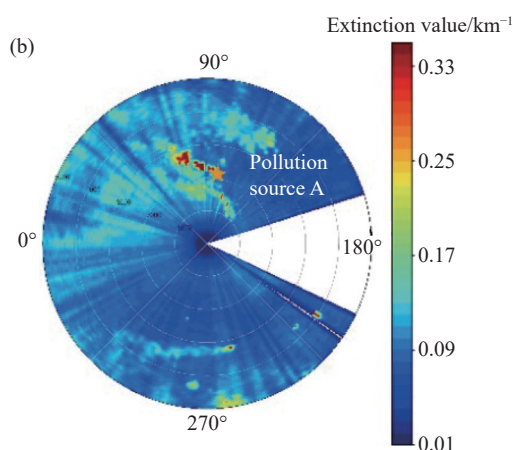


图 7 红外气溶胶激光雷达扫描监测结果(2月3日19:00-20:00)

Fig.7 Scanning and monitoring results of infrared aerosol lidar(February 3, 19:00 to 20:00)

所示。结果显示,激光雷达站点北面方向存在明显污染源,污染源位置为污染源A附近区域,该时段内地面主导风向为东南风,风速等级为1级,污染源A所产生污染物在东南风作用下,向西北方向扩散,而该国控站点不在污染源A的下风向,对国控站点颗粒物浓度数据未产生明显影响。同样国控站点数据显示

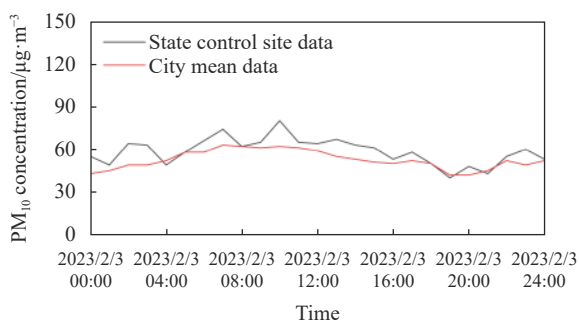


图 8 2月3日某市颗粒物浓度变化图

Fig.8 Time variation of particulate matter concentration on February 3

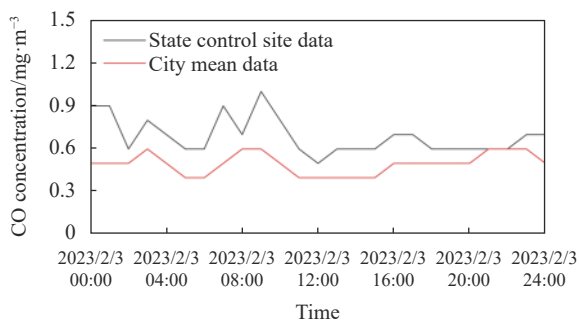


图 9 2月3日某市一氧化碳浓度变化图

Fig.9 Time variation of CO concentration on February 3

该时段内站点颗粒物小时浓度与市平均颗粒物浓度基本持平,未受到明显周边污染影响。

3.2 水平能见度监测应用个例分析

能见度定义为白天人们肉眼所能看见的水平天空背景下目标物(黑色、大小适度)轮廓的最远距离。目标物体辐亮度 L_O 与水平天空背景辐亮度 L_H 的相对误差可用对比度 C_V 来表示:

$$C_V = \frac{L_O - L_H}{L_H} \quad (8)$$

人们肉眼所能看见目标物时的最小对比度 C_V 称之为对比度阈值 ε ,在通常的天气条件下, $\varepsilon = 0.02$ 。故能见度也可定义为当物体相对与水平天空背景的对比度严格等于 ε 时该物体的距离。水平能见度 V_H 与大气水平消光系数 α_H 之间的关系如下^[17]:

$$V_H = \frac{1}{\alpha_H} \ln \frac{1}{\varepsilon} = \frac{1}{\alpha_H} \ln \frac{1}{0.02} = \frac{3.912}{\alpha_H} \quad (9)$$

式中: V_H 为大气水平能见度(单位:km); α_H 为消光系数(单位: km^{-1})。

两台能见度激光雷达与气象观测站前向散射能见度仪同期同址观测,观测时间段为3月24日22:00至3月27日17:00,时间分辨率为5 min。能见度激光雷达数据进行系数校准调试后,需对数据进行预处理,剔除粗大误差、点数平滑后进行比对。比对结果如图10、图11所示。两台能见度激光雷达变化趋势趋于一致,相关系数为0.98,相对误差7.76%,仪器性能较为稳定。两台能见度激光雷达与能见度仪同期数据比对分析相对误差分别为15.54%、13.84%,均小于20%,达到国际气象组织对能见度测量仪误差的要求,说明与标准数据一致性较好。监测期间能见度呈单峰分布,白天能见度相对较高,夜间能见度降低,

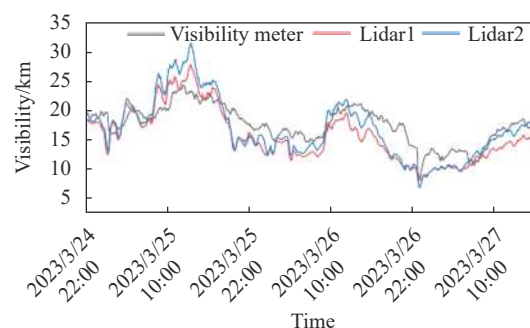


图 10 3月24日21:28至3月27日16:53能见度激光雷达比对结果

Fig.10 Visibility comparison results of infrared lidar from 21:28 on March 24 to 16:53 on March 27

25 日午间时间段能见度大于 25 km, 26 日至 27 日能见度降低, 结合环境空气质量分析, 颗粒物浓度由 25 日 $71 \mu\text{g}/\text{m}^3$ 增加至 26 日的 $131 \mu\text{g}/\text{m}^3$, 是能见度降

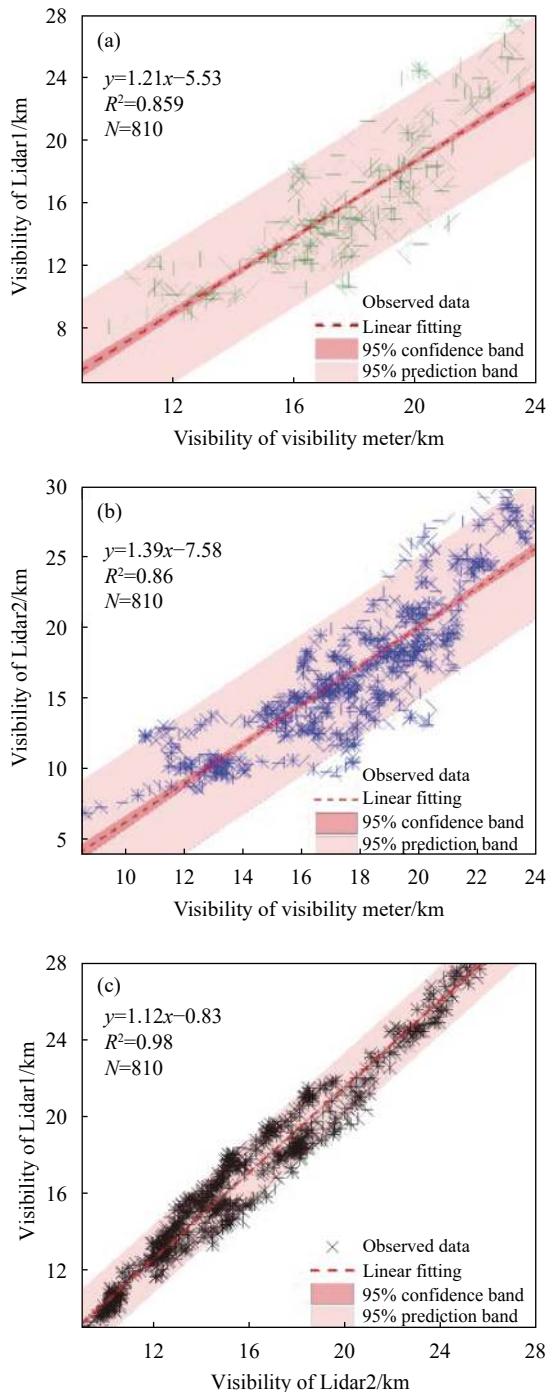


图 11 不同监测设备能见度数据线性回归分析。(a) 激光雷达 1 与能见度仪; (b) 激光雷达 2 与能见度仪; (c) 激光雷达 1 与激光雷达 2

Fig.11 Linear regression analysis of visibility of different equipment. (a) Lidar1 and visibility meter; (b) Lidar2 and visibility meter; (c) Lidar1 and Lidar2

低主要因素。

3.3 大气边界层监测应用个例分析

红外激光雷达与探空气球同址同期观测, 激光雷达时间分辨率为 10 min, 探空气球数据为每日 2 组, 早晚 8 时各一组。消光系数边界层高度计算方法为梯度法, 探空气球边界层高度计算方法为整体理查森数法^[18] 和 Liu 和 Liang^[19] 法。整体理查森数法计算前探空数据进行线性插值, 垂直高度分辨率加密为 20 m, 当总体理查森数 (R_i) 达到或超过临界理查森数 ($R_c=0.25$) 时, 将这一层的高度估算为边界层高度。但是该方法在计算上午边界层时会出现边界层过低的现象, 该种情况下采用 Liu 和 Liang 法计算。

能见度激光雷达与探空边界层高度比对结果如图 12 所示, 消光系数反演边界层高度绝对偏差为 200 m, 相关系数为 0.92, 如图 13 所示, 与探空气球计算的边界层高度具有一致性, 激光雷达数据通过梯度法能够较好的反演对流边界层高度。而夜间时间段激光雷达反演的边界层高度相对较高, 综合分析主要受到夜间污染残留层的影响, 并非夜间稳定边界层高度。

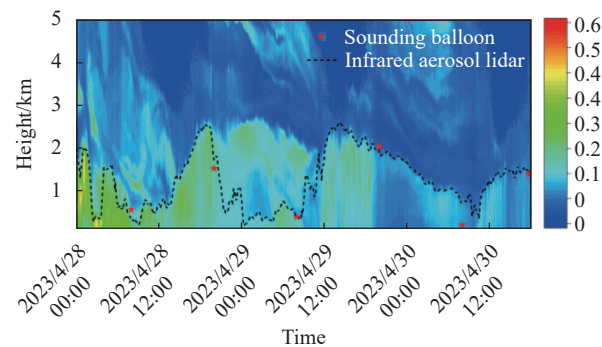


图 12 能见度激光雷达与探空边界层高度比对结果

Fig.12 Comparison of boundary layer height measured by visibility lidar and sounding balloon

监测期间边界层平均高度为 1.2 km, 与赵采玲等研究结论相符^[20]。边界层高度日变化趋势明显, 夜间边界层变化幅度相对小, 高度均低于 1 km, 而日出后开始扩展, 随着太阳辐射加强、近地面湍流运动的增强于午后扩展到最大值, 白天边界层平均高度 1.4 km。边界层高度是影响空气污染扩散的关键因素之一, 28 日与 29 日上午边界层低, 污染物不易扩散, 垂直对

流弱,消光系数大,30日边界层高于之前,扩散条件相对好,消光系数低,颗粒物影响程度弱。

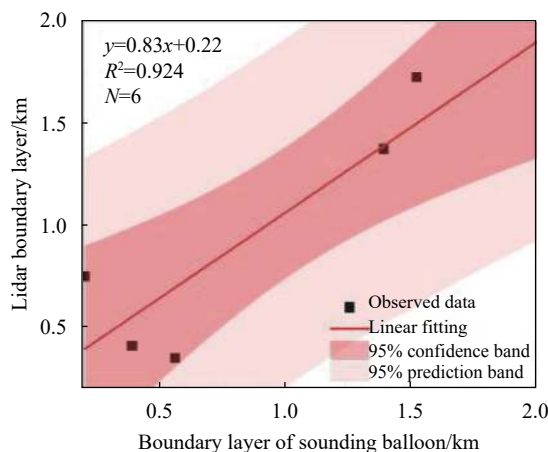


图13 能见度激光雷达与探空边界层高度相关性

Fig.13 Correlation between visibility Lidar and sounding boundary layer height

4 结论

文中研制一款全天时便携式户外型红外探测气溶胶激光雷达。采用1064 nm波长大气气溶胶监测结果更加准确,且结构紧凑,具有大气穿透性强,受阳光影响小、能够三维扫描等特点。通过实验分析,该雷达可有效应用于大气气溶胶污染时空分布特征获取、水平能见度监测、垂直边界层监测等领域,并取得较好成效。其具体应用结论如下:

1) 红外探测激光雷达水平扫描监测可及时发现区域内污染源,监测期间共发现10处主要污染源区域,分布在雷达点位的东南侧和东北侧区域。结合扫描区域内国家城市环境空气质量监测站点颗粒物浓度数据综合分析,污染源在东北风的作用下向西南扩散,导致下风向站点颗粒物和一氧化碳浓度同步大幅升高;而当主导风向为东南风时,污染源未对该站点数据造成显著影响。

2) 两台红外探测激光雷达与能见度仪同期同址观测,结果显示两台激光雷达能见度相关系数为0.98,相对误差7.76%,变化趋势一致,仪器性能较为稳定。与能见度仪数据比对分析相对误差均小于20%,与标准数据一致性较好。能见度日变化呈单峰分布,白天能见度较夜间高,26日至27日能见度降

低,结合环境空气质量分析,颗粒物浓度升高是影响能见度主要因素。

3) 红外激光雷达与探空气球同址同期反演边界层高度,结果显示,激光雷达边界层高度与探空气球绝对偏差为200 m,能够准确反演边界层高度。监测期间激光雷达反演的边界层高度存在日变化趋势,平均高度为1.2 km,而夜间时段边界层高度明显高于探空反演边界层高度,受到夜间污染残留的影响,并非夜间稳定边界层高度。

参考文献:

- [1] Spinhrne J D. Miero pulse lidar [J]. *Ieee Trans Geosci Remote Sens*, 1993, 31(1): 48-55.
- [2] Huang Zhongwei, Wang Yongkai, Bi Jiangrong, et al. An overview of aerosol lidar: Progress and prospect [J]. *National Remote Sensing Bulletin*, 2022, 26(5): 834-851. (in Chinese)
- [3] Wang Lin. Research of atmospheric aerosol lidar scanning technology[D]. Beijing: University of Chinese Academy of Sciences, 2006. (in Chinese)
- [4] Zhong Zhiqing, Zhou Jun, Qi Fudi, et al. Portable Mie lidar for monitoring atmospheric aerosol extinction [J]. *High Power Laser and Particle Beams*, 2003, 15(12): 1145-1147. (in Chinese)
- [5] Chen Chao, Wang Zhangjun, Song Xiaoquan, et al. Development and observational studies of scanning aerosol lidar [J]. *Infrared and Laser Engineering*, 2018, 47(12): 1230009. (in Chinese)
- [6] Lü Yang, Li Zhengqiang, Xie Jianfeng, et al. Monitoring the distributed point pollution sources based on a scanning lidar [J]. *China Environmental Science*, 2017, 37(11): 4078-4084. (in Chinese)
- [7] Wang Yaoting, Miao Shiguang, Zhang Xiaoling. Seasonal characteristics of the aerosol optical parameters based on lidar over the Beijing area [J]. *China Environmental Science*, 2016, 36(4): 970-978. (in Chinese)
- [8] Wang Yuesi, Gong Zhengyu, Liu Zirui, et al. Construction and application of comprehensive observation network for air pollution in Beijing-Tianjin-Hebei and its surrounding areas [J]. *Research of Environmental Sciences*, 2019, 32(10): 1651-1663. (in Chinese)
- [9] Chen Jing, Zhang Yanpin, Yang Peng, et al. Pollution process

- and optical properties during a dust aerosol event in Shijiazhuang [J]. *China Environmental Science*, 2016, 36(4): 979-989. (in Chinese)
- [10] Liu Jingle, Shi Jing, Li Peiyuan, et al. Study of atmospheric boundary layer height over Tianjin sea-shore-land area based on Lidar [J]. *China Environmental Science*, 2023, 43(10): 5070-5077. (in Chinese)
- [11] Winker D M, Hunt W H, McGill M J. Initial performance assessment of CALIOP [J]. *Geophysical Research Letters*, 2007, 34(19): L19803.
- [12] Huang Chunhong. Infrared micro-pulse lidar system development [D]. Qingdao: Ocean University of China, 2011. (in Chinese)
- [13] Wang Qiyu. Research on near infrared raman lidar for detecting atmospheric aerosol [D]. Xi'an: Xi'an University of Technology, 2020. (in Chinese)
- [14] Zhang Zhanye. Research on the control and inversion algorithm of the scanning lidar [D]. Hefei: University of Science and Technology of China, 2019. (in Chinese)
- [15] Chen Jianhua, Bo Yiyun, Li Peisheng, et al. Study on characteristics of air pollutant discharge from industrial pollution sources of Beijing city [J]. *Industrial Safety and Environmental Protection*, 2003, 29(2): 3-5. (in Chinese)
- [16] Guo Rui, Zhang Zhenjiang, Gao Wei. Application of lidar in atmospheric environment monitoring in Sanmenxia city [J]. *Chemical Engineering Design Communications*, 2019, 45(10): 243-244. (in Chinese)
- [17] Xie Chenbo, Han Yong, Li Chao, et al. Mobile lidar for visibility measurement [J]. *High Power Laser and Particle Beams*, 2005, 17(7): 971-975. (in Chinese)
- [18] Sorenson J H, Rasmussen A, Ellermann T, et al. Mesoscale influence on long-range transport -evidence from ETEX modelling and observations [J]. *Atmospheric Environment*, 1998, 32(24): 4207-4217.
- [19] Liu S, Liang X Z. Observed diurnal cycle climatology of planetary boundary layer height [J]. *Journal of Climate*, 2010, 23(21): 5790-5809.
- [20] Zhao Cailing, Li Yaohui, Liu Yuanpu, et al. The variation characteristics of planetary boundary layer height in northwest China: Based on radiosonde and ERA-Interim reanalysis data [J]. *Plateau Meteorology*, 2019, 38(6): 1181-1193. (in Chinese)

Design and application of all-day portable outdoor infrared detection aerosol lidar system

Zhuang Peng^{1,2}, Xie Chenbo³, Kang Baorong², Liu Jianming², Xia Xiaowei^{4*}

(1. School of Electrical Engineering, Tongling University, Tongling 244061, China;

2. Anhui Lanke Information Technology Co., Ltd., Hefei 230031, China;

3. Key Laboratory of Atmospheric Optics Anhui Institute of Optics and Fine Mechanics, Chinese Academy of Sciences, Hefei 230031, China;

4. School of Mechanical Engineering, Chaohu University, Hefei 238000, China)

Abstract:

Objective Air pollution control has higher requirements for environmental monitoring equipment. As an active remote sensing instrument, lidar is currently a powerful tool for monitoring the three-dimensional distribution characteristics of atmospheric aerosols in the troposphere. Lidar can compensate for the insufficient spatial distribution rate of existing ground monitoring data, mainly using various monitoring modes such as horizontal, vertical, navigation, and networking. Among them, horizontal scanning can effectively monitor horizontal visibility, dynamically extract the location and transmission path of pollution sources. Moreover, vertical monitoring can analyze the spatiotemporal changes in aerosol vertical diffusion, sedimentation transport, optical

characteristics, boundary layer changes and their cloud information, as well as sand and dust monitoring. This article introduces a self-developed infrared lidar that can detect aerosol distribution, visibility, and boundary layer height in real-time under environmental pollution and multiple sudden weather conditions. It has unique advantages in analyzing the diffusion and sedimentation trends of polluted air masses. In the context of increasing observation needs, it can provide more scientific and effective data support for environmental management decisions and meteorological services.

Methods The detection principle is based on the Mie scattering lidar equation. The schematic diagram and appearance of the aerosol lidar product structure are shown (Fig.2). The system mainly consists of three parts of laser emission unit, optical receiving unit, and data acquisition and processing unit. The main technical specifications are shown (Tab.1). The fundamental frequency 1 064 nm linearly polarized laser of Nd: YAG laser is used as the detection light source, and the telescope uses an aspherical lens as the main mirror. The aspherical lens has the advantages of small aberration and short focal length, which can reduce the volume of the receiving module. The subsequent optical and detection units are composed of fiber coupling devices and small core diameter multimode fibers, which can effectively control the telescope's receiving field of view. The optical channel measures the scattering signal generated by the interaction between 1 064 nm outgoing laser and atmospheric particles. By using the measurement data of the channel and combining with the above inversion method, the distribution characteristics of optical parameters of tropospheric aerosols and clouds can be obtained.

Results and Discussions This radar can be effectively applied in fields such as obtaining the spatiotemporal distribution characteristics of atmospheric aerosol pollution, monitoring horizontal visibility, and monitoring vertical boundary layers. The specific application conclusions are as follows.

1) Infrared detection lidar horizontal scanning monitoring can timely detect pollution sources in the area. During the monitoring period, a total of 10 main pollution source areas were discovered (Fig.3), distributed in the southeast and northeast sides of the radar points. Based on the comprehensive analysis of particulate matter concentration data from national urban environmental air quality monitoring stations within the scanning area, the pollution source spreads southwestward under the influence of northeast winds, resulting in a significant increase in particulate matter and carbon monoxide concentrations at downwind stations simultaneously.

2) Two infrared detection lidars were observed at the same location as the visibility meter, and the results showed that the correlation coefficient of visibility between the two lidars was 0.98, with a relative error of 7.76% (Fig.10-11). The trend of change was consistent, and the instrument performance was relatively stable. The relative error in comparison and analysis with the visibility meter data is less than 20%, which is consistent with the standard data. The daily variation of visibility shows a unimodal distribution, with higher daytime visibility compared to nighttime. From the 26th to the 27th, visibility decreases. Combined with environmental air quality analysis, an increase in particulate matter concentration is the main factor affecting visibility.

3) The infrared lidar and sounding balloon simultaneously inverted the boundary layer height, and the results showed that the absolute deviation between the lidar boundary layer height and the sounding balloon was 200 m, which can accurately invert the boundary layer height. During the monitoring period, the height of the boundary layer inverted by the lidar showed a diurnal trend, with an average height of 1.2 km (Fig.12). However, during the nighttime period, the height of the boundary layer was significantly higher than that of the sounding inversion,

which was affected by residual pollution at night and was not a stable boundary layer height at night.

Conclusions Infrared detection aerosol lidar has the characteristics of strong atmospheric penetration, little influence by sky background light, and sensitivity to large particles, and has achieved good results in the spatial and temporal distribution characteristics of atmospheric aerosol pollution, horizontal visibility monitoring, and vertical boundary layer monitoring. Horizontal scanning can obtain a map of particulate matter distribution in a large area, find pollution sources in time, and evaluate the impact of pollution sources by combining data such as wind speed, wind direction, particulate matter and carbon monoxide concentration near the ground. The system can accurately capture the distribution and transmission of atmospheric aerosols in real time, and accurately invert information such as horizontal visibility and boundary layer height, and has a wide range of application scenarios in the field of atmospheric parameter monitoring.

Key words: infrared aerosol lidar; particulate matter distribution; visibility; boundary layer

Funding projects: Natural Science Foundation of Anhui Province (2208085UQ03); Collaborative Innovation Program of Hefei Science Center, Chinese Academy of Sciences(2022HSC-CIP025); Talent Project of Chaohu University (KYQD-2023056)